

Thunderstorms in Hawaii

AC .H3 no.L68

15393



Lee, Clarence B. H.
SOEST Library

THESIS

070
Lee
Thu
ms

THUNDERSTORMS IN HAWAII

**A THESIS SUBMITTED TO THE GRADUATE DIVISION OF THE
UNIVERSITY OF HAWAII IN PARTIAL FULFILLMENT
OF THE REQUIREMENTS FOR THE DEGREE OF
MASTER OF SCIENCE
IN GEOSCIENCES - METEOROLOGY
JUNE 1968**

By

Clarence B. H. Lee

Thesis Committee:

**Colin S. Ramage, Chairman
Edwin F. Danielsen
Alfred H. Woodcock**

**RETURN TO
HAWAII INSTITUTE OF GEOPHYSICS
LIBRARY ROOM**

We certify that we have read this thesis and that
in our opinion it is satisfactory in scope and quality as
a thesis for the degree of Master of Science in
Geosciences - Meteorology.

THESIS COMMITTEE

Chairman

TABLE OF CONTENTS

ABSTRACT	ii
LIST OF TABLES	iv
LIST OF FIGURES	vi
INTRODUCTION	1
DISCUSSION OF METHODS AND RESULTS	5
Frontal Days	5
Cyclone Days	7
Map Types	11
Temperatures	15
Temperature Changes	18
Vertical Motion	18
Diabatic Effects	19
Advection	23
Stability	25
Relative Humidity	29
Physical Modeling	34
CONCLUSIONS	48
RECOMMENDATIONS	51
APPENDIX	64
BIBLIOGRAPHY	65

LIST OF TABLES

Table 1.	Frequency of frontal-days with thunderstorm-days	6
Table 2.	Frequency of cyclone-days with thunderstorm-days	10
Table 3.	Frequency of thunderstorm days with map types	13
Table 4.	Mean 700 and 300 mb temperature at Lihue	16
Table 5.	Frequency of thunderstorm-days with 700 mb temperatures at Lihue	17
Table 6.	Frequency of thunderstorm-days with 300 mb temperature at Lihue	17
Table 7.	Average advective temperature tendency at Lihue	24
Table 8.	Input parameters for cumulus dynamics cloud model 1500 GMT 15 Jan 57	44
Table 9.	Input parameters for cumulus dynamics cloud model 1500 GMT 16 Jan 57	45
Table 10.	Input parameters for cumulus dynamics cloud model 1500 GMT 17 Jan 57	46
Table 11.	Input parameters for cumulus dynamics cloud model 0300 GMT 8 Feb 56	52
Table 12.	Input parameters for cumulus dynamics cloud model 0300 GMT 9 Feb 56	54

Table 13.	Input parameters for cumulus dynamics	
	cloud model 0300 GMT 10 Feb 56	56
Table 14.	Input parameters for cumulus dynamics	
	cloud model 1500 GMT 17 Feb 56	58
Table 15.	Input parameters for cumulus dynamics	
	cloud model 1200 GMT 20 Jan 62	60
Table 16.	Input parameters for cumulus dynamics	
	cloud model 0000 GMT 22 Jan 62	62
Table 17.	Input parameters for cumulus dynamics	
	cloud model 1200 GMT 28 Jan 62	63

LIST OF FIGURES

Figure 1.	Monthly Distribution of Thunder- storm-days	2
Figure 2.	Diurnal Thunderstorm Distribution . . .	3
Figure 3.	Diurnal Lightning Distribution	4
Figure 4.	Areas for Fronts and Cyclones	8
Figure 5.	Map Types	12
Figure 6.	Radiative Cloud Schematic	20
Figure 7.	Virtual-equivalent-potential Temperature, 7-18 Feb 56	26
Figure 8.	Virtual-equivalent-potential Temperature, 15-20 Jan 57	27
Figure 9.	Virtual-equivalent-potential Temperature, 19-31 Jan 62	28
Figure 10.	Relative Humidity, 7-18 Feb 56	30
Figure 11.	Relative Humidity, 15-20 Jan 57	31
Figure 12.	Relative Humidity, 19-31 Jan 62	32
Figure 13.	Steady State Flow Diagram	37
Figure 14.	Cloud Heights vs. Updraft Radius, 8-10, 17 Feb 56	39
Figure 15.	Cloud Heights vs. Updraft Radius, 15-17 Jan 57	40
Figure 16.	Cloud Heights vs. Updraft Radius, 15-17 Jan 57	41
Figure 17.	Cloud Heights vs. Updraft Radius, 20, 22, 28 Jan 62	42

ABSTRACT

Thunderstorm occurrences are compared with synoptic patterns (proximity of fronts, cyclones, and flow patterns). Only very small numbers of thunderstorms are found to be associated with these large scale patterns.

The relationship of diabatic effects, convection, and horizontal advection to temperature changes is discussed and some computations are compared with observed data. It is found that the advective tendency is not related to the observed temperature changes. The observed changes probably result from compensating effects produced by non-adiabatic and convective influences which may be an order of magnitude larger than the advective contribution. The orders of magnitude of convective cooling and radiative cooling at cloud tops are estimated by calculations. Although the models are crude, they indicate that vertical motion is the most important destabilizing influence.

Some case studies of air-mass structure are made through the use of virtual-equivalent-potential temperature and relative humidity time sections. Soundings are found to be convectively unstable at all times, despite the presence of the trade inversion above the moist layer, but thunderstorms are more prevalent when the moist layer is deep and the trade inversion is weak or non-existent. Since a relatively small amount of lifting is necessary to release the convective instability the mountainous terrain would

produce frequent thunderstorms unless cumulus development is strongly inhibited by other, perhaps related, conditions. Entrainment of dry air has the desired effect, but numerical computations based on a model which simulates cumulus dynamics including entrainment show that entrainment is a necessary but not sufficient condition to explain the relatively infrequent occurrences of thunderstorms.

THUNDERSTORMS IN HAWAII

INTRODUCTION

The annual and semi-diurnal thunderstorm frequencies (Figs. 1-3) in the Hawaiian Islands have been described by Lee (1967). These frequencies revealed marked periodicities suggesting more than casual relationships with both synoptic and microscale phenomena. Thunderstorm occurrences are highest during the cool months from October through March. The frequency generally attains a maximum during March. This seasonal variation suggests a correlation with the more common wintertime disturbances, viz., fronts and cyclones. It was shown also that the diurnal thunderstorm frequency is bimodal in structure, having distinct maxima during the mid-afternoon and early morning hours. The earlier study suggested radiative cooling as a probable factor in the production of the nocturnal maxima.

In the present study the suggested relationships between thunderstorms and large scale synoptic features are first examined statistically. When one or more thunderstorms or lightning is reported at either Lihue, Honolulu, or Hilo the day is classified as a "thunderstorm day". The number of thunderstorm and non-thunderstorm days is then determined when fronts, and cyclones are in proximity to these stations. The numbers are also determined for typical flow patterns. The inference of cold advection aloft as an initiator of thunderstorms leads to a discussion of the relationship of

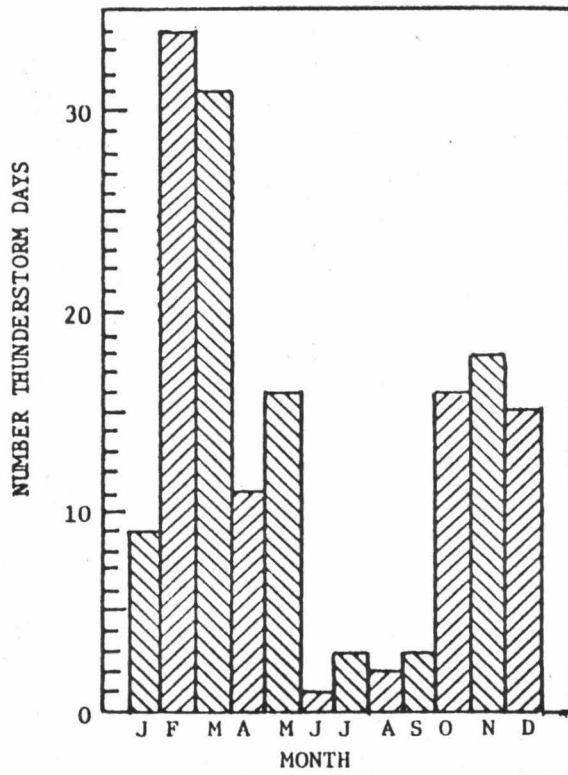


Fig. 1a. Hilo - Feb 1946-Aug 1966

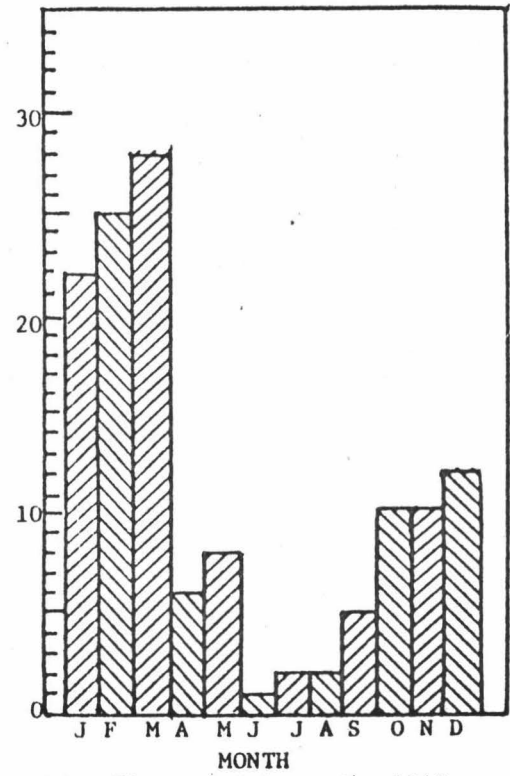


Fig. 1b. Honolulu - Jan 1948-Sept 1966

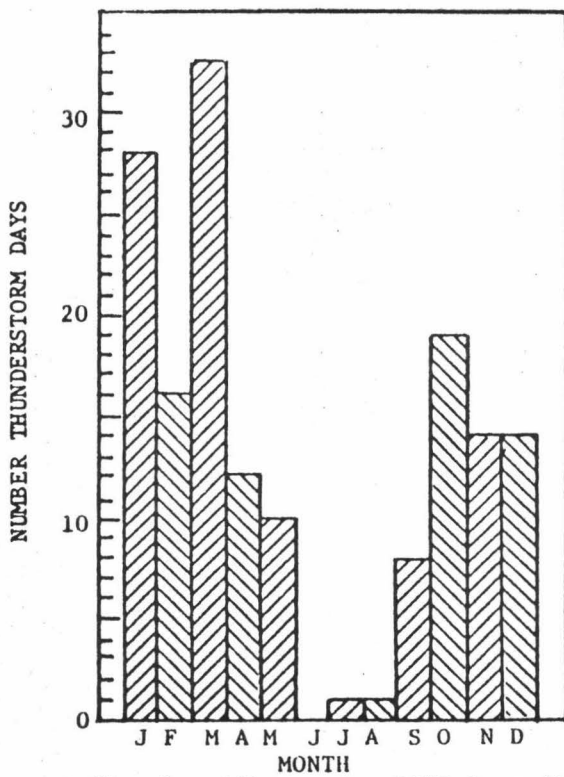


Fig. 1c. Lihue - Jan 1950-Sept 1966

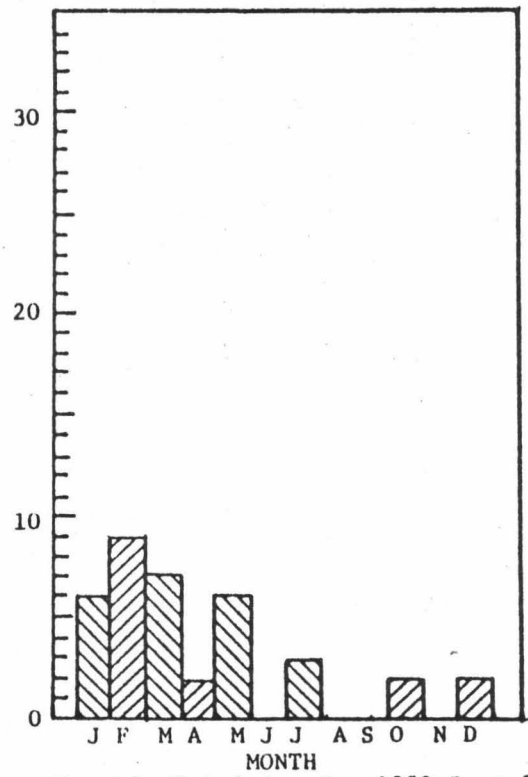


Fig. 1d. Kahului - Jan 1959-Sept 1966

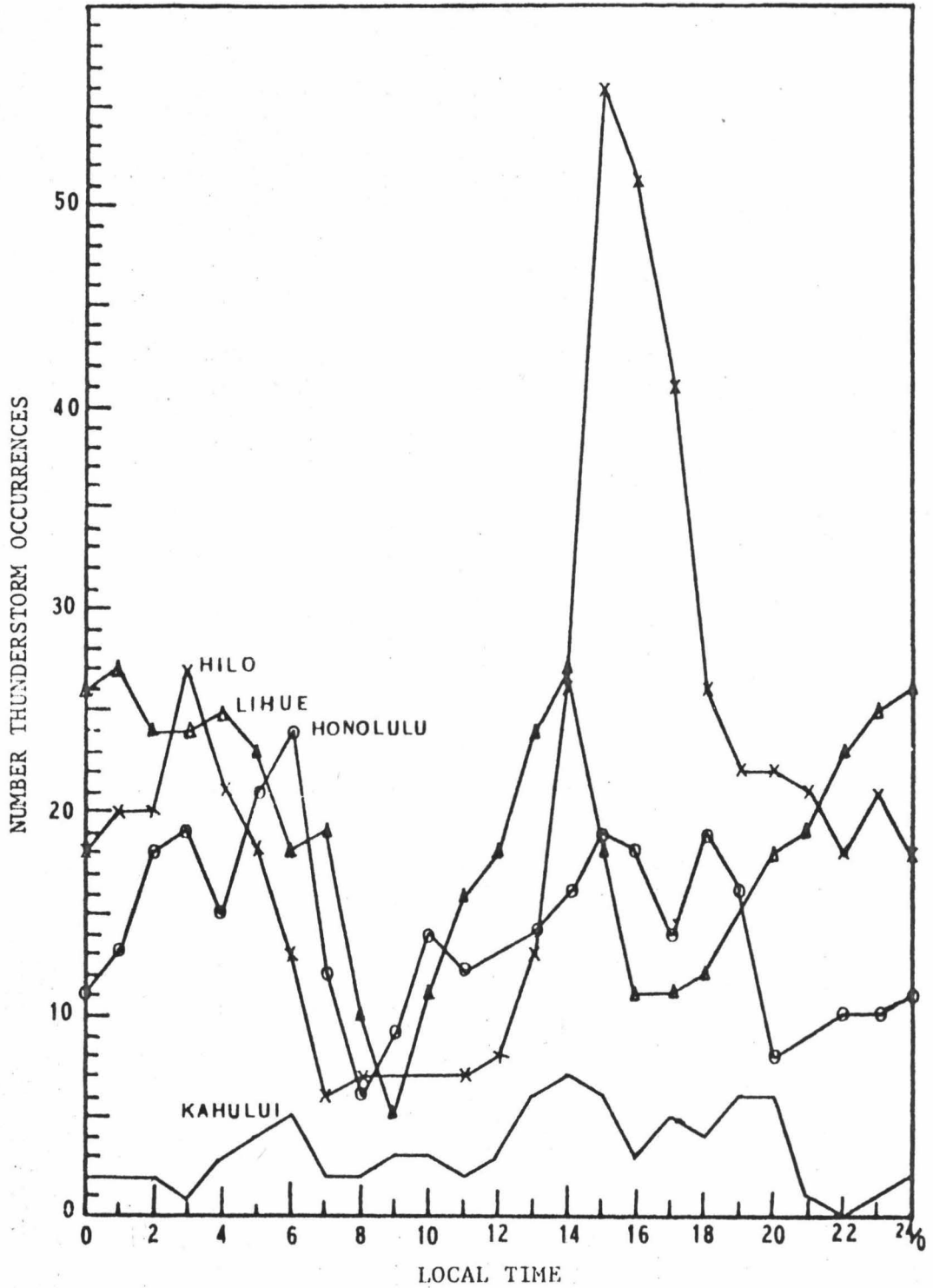


FIG. 2. DIURNAL THUNDERSTORM DISTRIBUTION

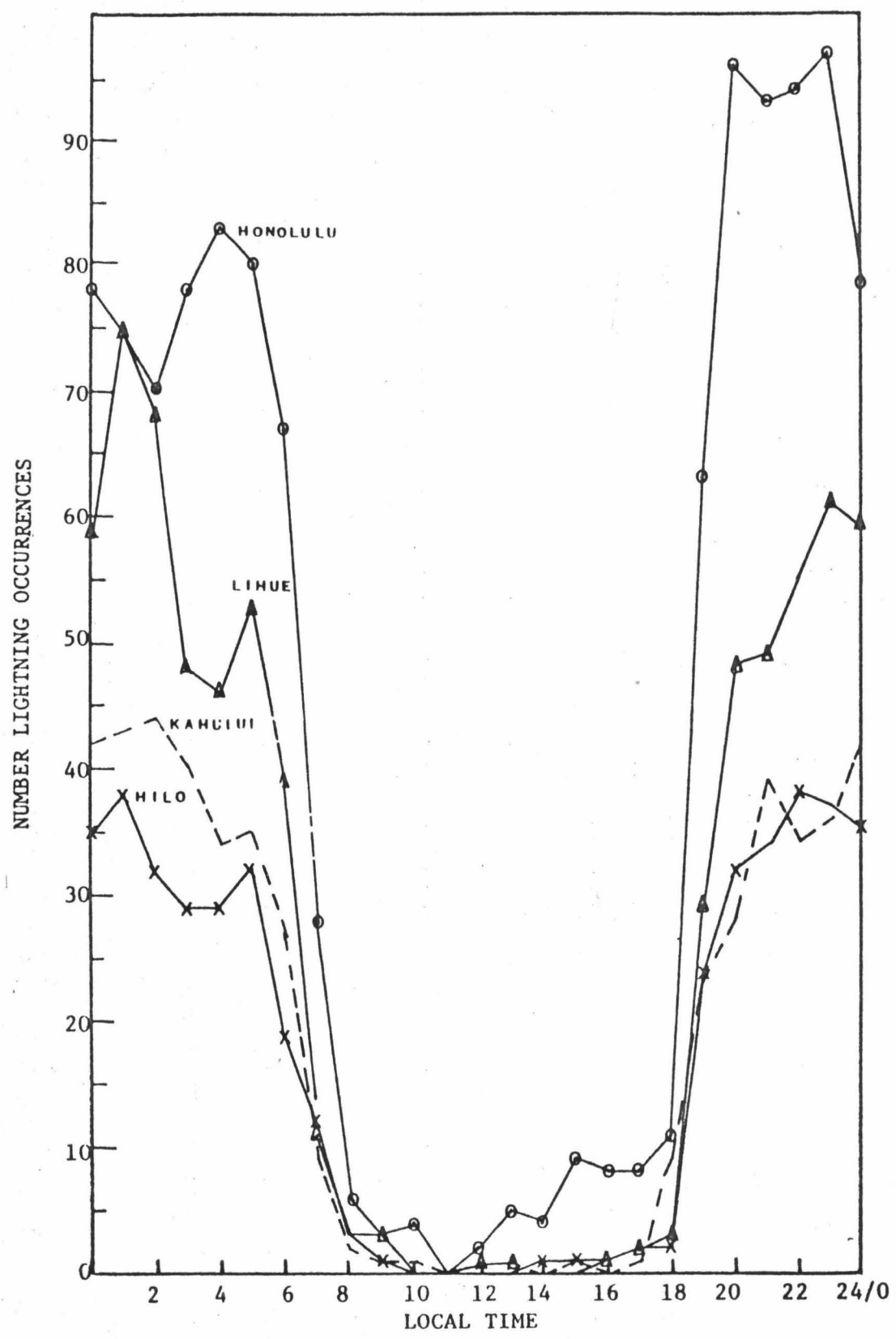


FIG. 3. DIURNAL LIGHTNING DISTRIBUTION

vertical motion, radiation, and horizontal advection to temperature changes. Estimates are made of the relative orders of magnitude of these three factors. Next, investigation of the vertical structure of the air mass, through the use of virtual-equivalent-potential temperature and relative humidity diagrams, reveals highly favorable conditions for thunderstorms but only infrequent occurrences. The relative rarity of thunderstorms suggests entrainment as a probable factor suppressing the production of more frequent thunderstorm activity. This suggestion is tested through the use of a numerical model which simulates cumulus dynamics and the effects of entrainment.

DISCUSSION OF METHODS AND RESULTS

FRONTAL DAYS

An analysis of frontal cloud bands from 20-30N and 155-180W taken from satellite nephanalyses during the period 1965-66 showed average frontal cloud widths of about 350 km. The rectangular area shown in Fig. 4 is chosen slightly larger to account for some variability and to include all of the Hawaiian chain. Frontal-days, i.e., when the mean position of the front is within the area (Worthley, 1967), are tabulated against the occurrence or non-occurrence of thunderstorm-days.

The results are shown in Table 1. Of a total of 618 frontal-days thunderstorms or lightning were reported on

Month	No. of frontal-days with a thunderstorm-day	No. of frontal-days without a thunderstorm-day	Total
Sep	3	10	13
Oct	9	40	49
Nov	6	57	66
Dec	18	89	107
Jan	22	126	148
Feb	7	80	87
Mar	22	53	75
Apr	5	53	58
May	5	11	16
Jun	0	2	2
Total	97	521	618

Table 1. Frequency of frontal-days with thunderstorm-days at Lihue, Honolulu or Hilo. Jan. 1950-Sept. 1966.

7

only 97 days or about 16 per cent of all cases. The ratio of thunderstorm-days to frontal-days during November is 1:11, December 1:6, January 1:7, February 1:12, March 1:3, and April 1:12. March, which has the highest ratio, is the month of peak thunderstorm frequency at Lihue and Honolulu. January contained nearly twice as many frontal-days as March, yet it experienced less than half the frequency of thunderstorm-days. A similar unexpected feature is observed in the low frequency of thunderstorm-days during February as compared to March although the number of frontal-days were similar.

CYCLONE DAYS

The remaining thunderstorm-days, when fronts were not present, are compared with days when cyclones were reported in the vicinity of the Hawaiian Islands (Worthley, 1967). The area chosen is larger than that for the fronts (see Fig. 4). When cyclones were analyzed in the area on one or more of the following levels, surface, 700, 500, and 300 mb, the day is classified as a "cyclone-day". If the cyclone was present at more than one level only the lowest level was used in the statistics.

Except for a few cases, Worthley determined that fronts and cyclones were mutually exclusive within a radius of about 500 miles of the island chain.

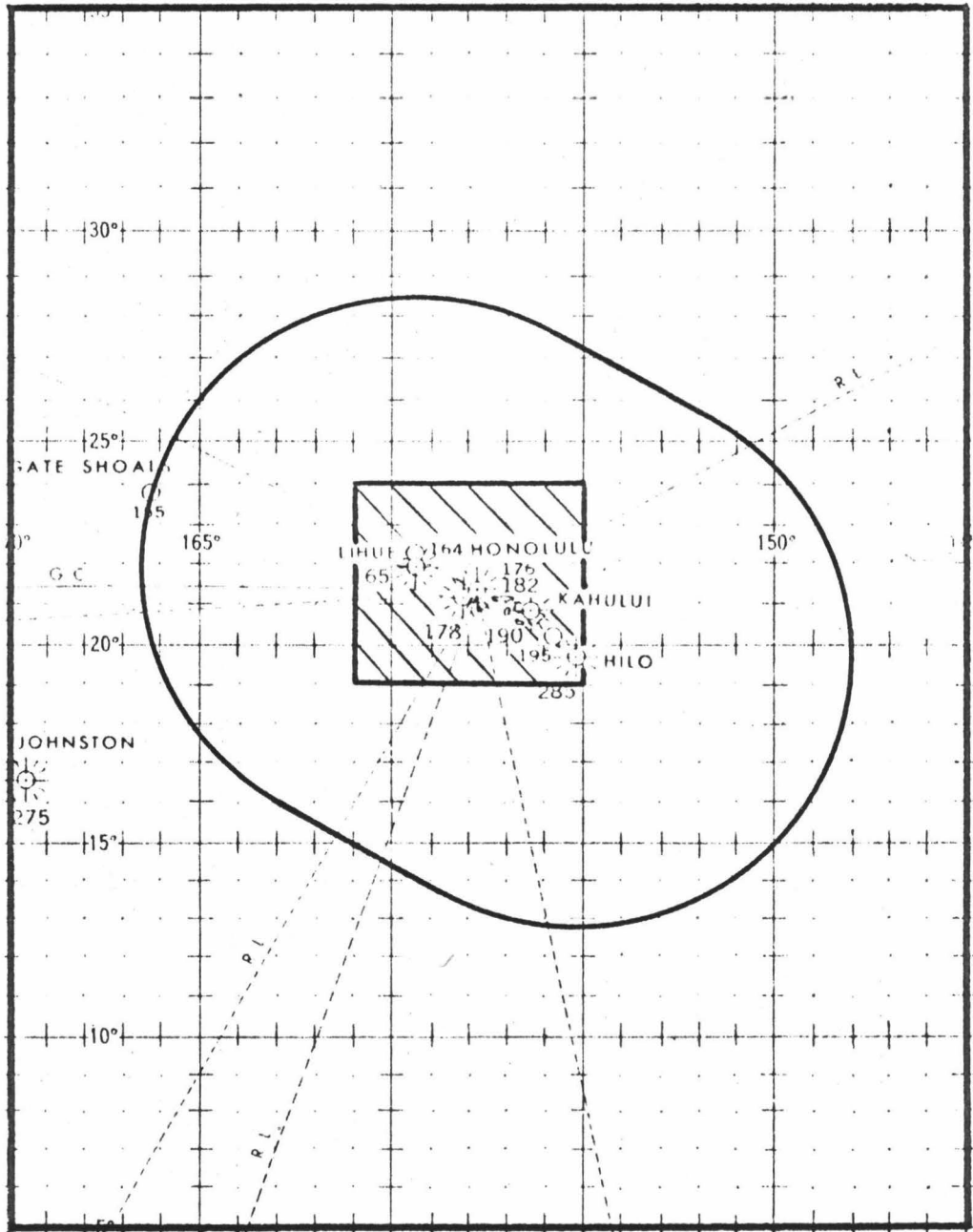


Fig. 4. Areas for fronts (hatched) and cyclone (elliptical) tabulations.

9

Table 2 shows the frequency distribution of thunderstorm-days with cyclones at various pressure surfaces. Of a total of 623 cyclone-days thunderstorms or lightning were reported on only 138 days or about 22 per cent of all cases. The table shows that thunderstorm-days are most frequent with cyclones at the surface (61 days out of 146). This undoubtedly reflects the influence of friction induced low level convergence. Friction induced low level convergence may provide sufficient vertical motions to release convective instability. In addition, the low level convergence is probably associated with vertical stretching which increases the lapse rate and increases buoyancy. Thunderstorm-day frequencies decrease progressively when the closed circulations are only observed aloft, with the exception of a relatively high frequency at 300 mb. This high frequency is due to the small number of cases when cyclones at 300 mb were not associated with cyclones at lower levels. This in turn may be due to the lack of data, since most of the analyses were performed prior to the era of jet transport.

The table suggests that lows aloft are inefficient producers of severe convective activity. Although the mid-tropospheric disturbances may produce convergence and rising motions above the level of the disturbance, the vertical motion field below is apparently characterized by subsidence.

Month	No. of Cyclone-days								Total
	with a thunderstorm-day				without a thunderstorm-day				
	300mb	500mb	700mb	Sfc	300mb	500mb	700mb	Sfc	
Jan	1			5	1	3		9	19
Feb	1	1	5	12		9	1	13	42
Mar	1	2	2	16		9	2	15	47
Apr		3	2	3	1	4	3	6	22
May		6	8	2	1	20	19		56
Jun		4	1	2	3	50	11	3	74
Jul		2	4		2	42	36	2	88
Aug		5				42	22	4	73
Sep		6	2	5	1	30	16	7	67
Oct	3	7	5	8		19	14	7	63
Nov		1		5	6	4	12	11	39
Dec		2	3	3	2	14	1	8	33
Total	6	39	32	61	17	246	137	85	623

Table 2. Frequency of cyclone-days with thunderstorm-days at Lihue, Honolulu or Hilo Jan. 1950-Sept. 1966. Blanks indicate no occurrence. Pressure levels indicate lowest pressure surface at which the closed circulation existed.

11

Over the Hawaiian Islands, peak activity with mid-tropospheric cyclones (but minimum thunderstorm activity) is observed during the summer months (Worthley, 1967). During this period the prevailing low level, subsiding easterly flow from the subtropical ridge north of the island chain is then overlain by high level westerlies.

MAP TYPES

The final comparison with synoptic-scale patterns was made using the classification system of Yeh et al (1951) and modified by Worthley (1967). In this comparison, each thunderstorm-day during the period is tabulated against the prevailing map type. The number of years of data is slightly reduced from the number used in the previous two sections, due to the non-availability of data. In addition, only the months of October-March are considered since the bulk of thunderstorm activity is observed during this period.

Table 3 lists the results of this comparison and Fig. 5 depicts the map type classifications. Table 3 shows that thunderstorms occurred most frequently with type 5, corresponding to the classical "Kona" patterns. However, significant contributions were also made by types 1a and 1b. While it could be expected that type 5 would be significantly related with thunderstorms, it is interesting to note the amount of activity associated with types 1a and 1b, both normally associated with tradewind (i.e. northeast to east) surface flow over the islands. The large number of thunder

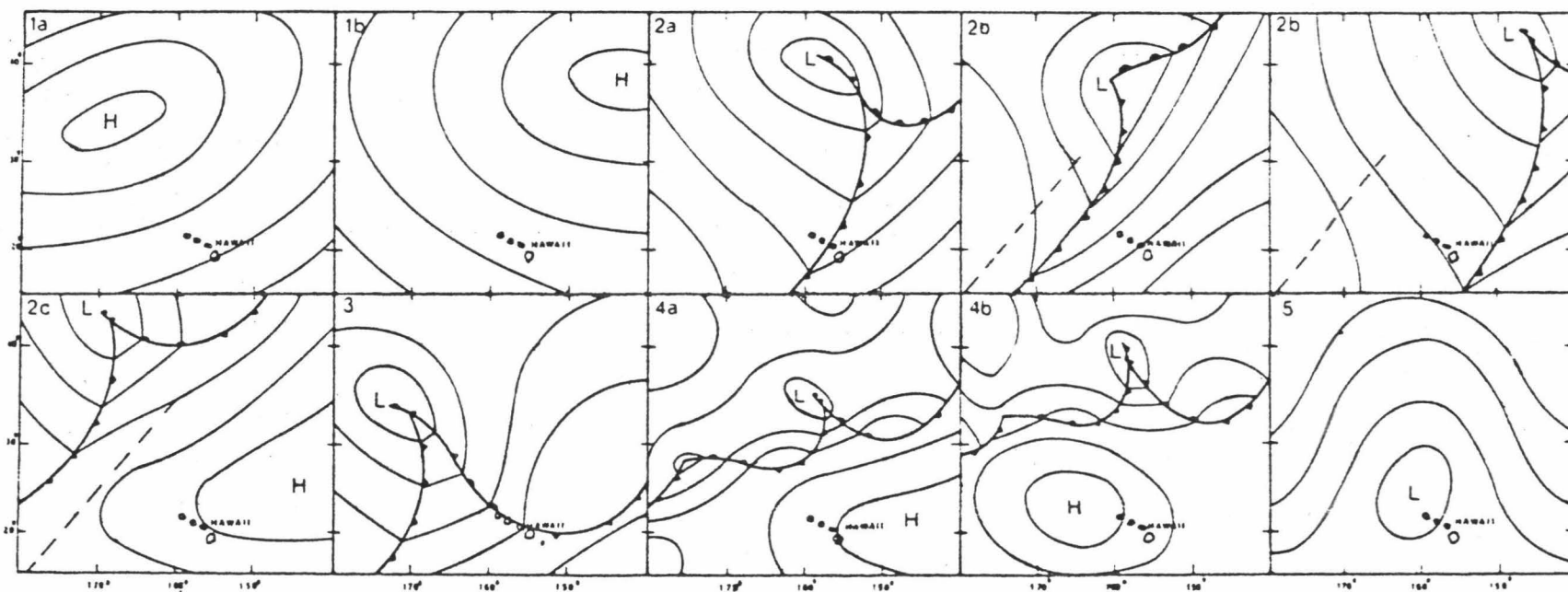


Fig. 5. Map types after Yeh *et al.* (1951).
(Type 2c added.)

Map Type	1a	1b	2a	2b	2c	3	4a	4b	5	Total
Total No. for period	517	560	166	450	311	6	210	12	161	2393
No. with thunderstorm-day	56	75	25	63	31	2	15	0	85	352
Percent of total with thunderstorm-day	11	13	15	14	10	33	7	0	53	100
Percent of total thunderstorm-days	16	21	7	18	9	1	4	0	24	100

Table 3. Frequency of thunderstorm-days with map types (after Yeh et al (1951) and Worthley (1967)) Oct.-Mar. 1950-55, Oct.-Mar. 1958-64, Jan. 1966.

storms associated with the tradewinds may indicate the influence of topographic lifting in generating cumulonimbus, but it is also interesting to note that the percentage of tradewind days with thunderstorms is low. Types 1a and 1b, reflecting the more frequent synoptic patterns over the islands, account for about 45 per cent of all map types. Only 11 per cent of type 1a patterns, however, were accompanied by thunderstorm-days; for type 1b, only 13 per cent. Types 2a and 2b individually and collectively were correlated with thunderstorm-days only slightly more than 14 per cent of the time, while type 2c had a frequency of only seven per cent. Type 5, the category most significantly related to thunderstorms, has a frequency of 53 per cent.

Interestingly, types 1a, 1b, 2b, and 5 have roughly similar frequencies of the total number of thunderstorm-days (16, 21, 18, and 24 per cent, respectively). Collectively, types 1a and 1b accounted for 37 per cent of the total number of thunderstorm-days while the frequency for type 5 was only 24 per cent; the remaining 39 per cent is accounted for by all other types combined.

The table shows that, while thunderstorms occur relatively infrequently with all map types (with the exception of map type 5), nearly four out of ten of all thunderstorm-days take place during the so-called tradewind patterns.

TEMPERATURES

In the course of the investigation, it was observed that thunderstorms occurred more often with cooler than normal temperatures aloft, particularly at 300 mb. This tendency suggested cold advection aloft as a possible initiator of thunderstorms. In order to test the apparent relationship of thunderstorms with temperatures aloft, mean temperatures at 300 mb and 700 mb over Lihue, Kauai for the months October-March were computed and thunderstorm-days at Lihue, Honolulu, or Hilo were tabulated against the occurrence of temperatures higher or lower than the means. The tabulations were made separately for 300 mb and 700 mb and for each month.

Tables 4-6, summarizing the results, show that thunderstorms do occur more frequently with cooler than normal temperatures aloft. The contingency tables indicate statistically significant values of chi-squared. However, it is clear from the tables that, while the probability of thunderstorms is enhanced by cooler than normal temperatures aloft, attempts at temperature correlation would be of little practical significance for forecasting thunderstorms. The problem is rendered more difficult since it is impossible to recognize whether the cooling is in response to advection, vertical motion, or diabatic effects.

Month	\bar{T}_{700}	s_{700}	\bar{T}_{300}	s_{300}
Jan	6.4	2.5	-36.3	3.6
Feb	5.8	2.8	-35.4	3.9
Mar	4.7	2.2	-38.2	3.3
Oct	7.7	2.2	-34.3	1.9
Nov	7.3	2.5	-36.1	2.1
Dec	6.8	2.4	-36.7	2.8

Table 4. Mean (barred) 1200 GMT 700mb and 300mb temperatures ($^{\circ}\text{C}$) and standard deviations(s) for Lihue 1958, 1960-63. Subscripts denote pressure levels.

	\bar{T}_{700}	\bar{T}_{700}	Sum
Thunderstorm occurred	95(60)	35(70)	130
No thunderstorm	326(361)	451(416)	777
Sum	421	486	907

chi-squared = 44.0

Table 5. Frequency of thunderstorm-days at Lihue, Honolulu or Hilo with Lihue mean 700mb temperature (Table 4) Oct.-Mar. 1958, 1960-63. No relation values in parantheses.

	\bar{T}_{300}	\bar{T}_{300}	Sum
Thunderstorm occurred	84(62)	45(68)	130
No thunderstorm	350(372)	428(405)	777
Sum	434	473	907

chi-squared = 17.5

Table 6. Frequency of thunderstorm-days at Lihue, Honolulu or Hilo with Lihue mean 300mb temperature (Table 4) Oct.-Mar. 1958, 1960-63. No relation values in parentheses.

TEMPERATURE CHANGES

From the earlier study it was evident that the marked semi-diurnal periodicity of Hawaiian thunderstorms required a systematic investigation of temperature changes and the methods by which they are produced.

The local time rate of change of temperature can be expressed primarily as a function of three major components and is shown by the relationship

$$\frac{\partial T}{\partial t} = \frac{1}{c_p} \frac{dq}{dt} - \nabla \cdot \nabla T - w(\gamma_d - \gamma) \tag{1}$$

(Definitions of the various symbols in this and subsequent equations are contained in the appendix.)

The first term of (1) represents the contribution due to non-adiabatic effects. The second term is the advection term and the last represents changes due to ascent or descent.

Vertical Motion

Calculations show that modest values of vertical motion can produce significant temperature changes. It can be shown by (1) that an updraft of six cm/s, acting alone, will produce changes in the order of one °C/hr. However, vertical motion is difficult to determine objectively and it is never routinely observed.

Diabatic Effects

Radiative heating and cooling, and latent heat release, are two of the important factors in the diabatic term of (1). Although many texts and articles allude to the efficacy of cloud top cooling in the production of nocturnal thunderstorms, very few contain a quantitative treatment.

In the absence of insolation and of other dynamic or thermodynamic mechanisms long-wave flux will cool the upper part of the cloud (see Fig. 6). Assuming an exponential decay rate with depth, the cooling rate at any level within the cloud can be expressed as

$$\left(\frac{dT}{dt}\right)_x = \left(\frac{dT}{dt}\right)_0 e^{-\alpha x} \tag{2}$$

where the depth is measured downward from the top of the cloud. Since the decay is exponential, if a value of one per cent is ascribed to the base of the layer with respect to the cloud top, then

$$1 = 100 e^{-\alpha x}$$

and

$$\left(\frac{dT}{dt}\right)_x = \left(\frac{dT}{dt}\right)_0 e^{-10^{-4} x} \tag{3}$$

The order of magnitude of α would remain essentially unchanged if the cooling rate at the bottom of the cloud layer with respect to the top of the cloud is assumed one order of magnitude smaller or larger than one per cent. This can be verified by substitution.

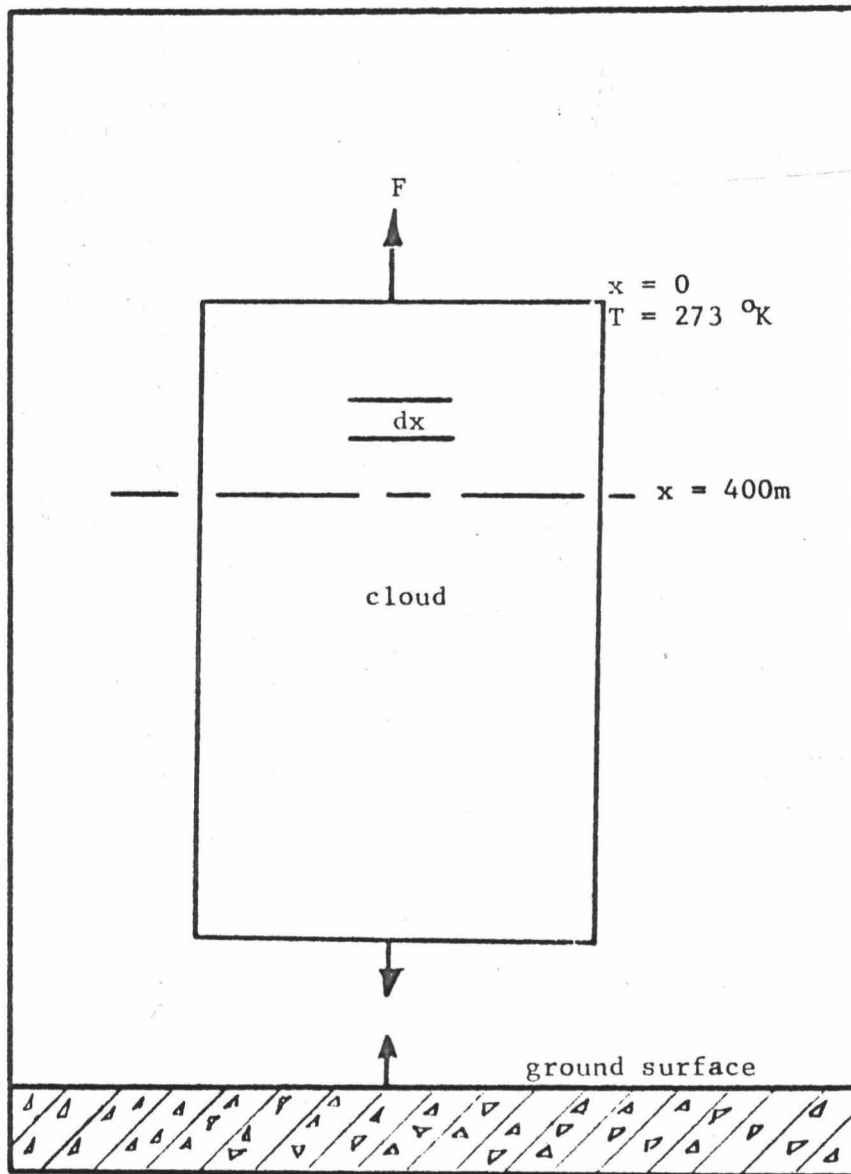


Fig. 6. Schematic of radiative cloud model

Neglecting other sources, the energy balance through the layer can be expressed as a relationship between the radiative flux and the sensible and latent heat losses as a consequence of cooling.

$$\int dx \left[c_p \frac{dT}{dz} + L \frac{dw}{dz} \right] = dF \tag{4}$$

Equation (4) can be shown in the alternate form

$$\int dx \frac{dT}{dz} \left[c_p + L \frac{e}{p} \frac{de}{dT} \right] = dF \tag{5}$$

The quantity within the brackets is insensitive to small changes and can be evaluated by tables or the Clausius-Clapyron equation and can be shown to be

$$c_p + L \frac{e}{p} \frac{de}{dT} \sim 0.5 \text{ cal/g}^{-1} \text{ } ^\circ\text{C}^{-1} \tag{6}$$

Thus, (3) and (5) can be combined. Substituting for (6) the relationship becomes

$$0.5 \int dx \left(\frac{dT}{dz} \right)_0 e^{-10^{-4}x} = dF \tag{7}$$

Since $\left(\frac{dT}{dz} \right)_0 \neq f(x)$, integrating from base to top of the layer,

$$\left(\frac{dT}{dz} \right)_0 = - \frac{F(10^{-4})}{0.5p} \tag{8}$$

Tabulations of F derived from the Stefan-Boltzman Law show that

$$F \sim 0.4 \text{ cal/cm}^2\text{min}^{-1}$$

Assuming an average value of $\rho = 10^{-3} \text{ g/cm}^3$ and that the ratio of net flux to total flux leaving the cloud top is one-half due to back radiation and solving (8), then,

$$\left(\frac{dT}{dt}\right)_0 = -2.4 \text{ }^\circ\text{C/hr}^{-1}$$

This amount of cooling is significantly large to be an important, if not decisive, factor in promoting or maintaining overturning. It is recognized that other considerations such as convection and long-wave flux through the bottom and sides of the layer have been neglected.

Similar estimates can be made of warming occurring at the base of the cloud due to long-wave flux originating from the ground. Consider a cloud base 1000 feet above ground with temperature 295 °K and surface temperature of 300 °K. Because of the small temperature difference the cloud flux differs only slightly from the flux originating at the ground. The effective net flux impinging on the cloud base, allowing for absorption in the layer between ground and cloud, is only about 0.025 cal/cm²/min. A calculation would indicate roughly one order of magnitude smaller than the value calculated above for cloud top cooling.

During the daytime the effect of insolation, assuming a cloud albedo of 80 per cent and effective incoming short-wave radiation of one langley/min, would completely cancel the upward flux through the tops of the cloud resulting in no cooling at cloud top.

Advection

The horizontal advection of temperature is simple to determine objectively. Utilizing the thermal wind and barometric equations it can be shown that

$$-\nabla_j \cdot \bar{\nabla}_p T = -2 \left[\frac{g}{R} \left(\ln \frac{p_1}{p_2} \right)^{-1} \left(\frac{1}{2} V_1 V_2 \sin \theta \right) \right] \quad (9)$$

The relationship shows that the horizontal advection is proportional to twice the area enclosed by the wind vectors.

Table 7 depicts the mean values of the advective tendency for the period 0300 GMT 10 Feb to 1500 GMT 18 Feb 56 computed by (9). The computations were made for 50 mb layers from 1000 to 200 mb. In general, mean advective tendencies are of the order 10^{-2} °C/hr.

The previous sections have shown that vertical motions and diabatic effects can have orders of magnitude of one °C/hr. The advective tendency is at least one order of magnitude less than one °C/hr. The comparison indicates that the actual temperature changes result primarily from two interacting factors. The dominant factor cannot be positively identified at any particular time.

P(mb)	$-(\bar{V} \cdot \bar{\nabla} T) \times 10^{-2} \text{ } ^\circ\text{C/hr}$	
	0300 GMT	1500 GMT
1000	9.7	20.2
950	12.6	21.2
900	7.2	17.3
850	6.1	19.8
800	7.9	-14.8
750	9.7	34.6
700	15.9	- 9.4
650	- 7.6	- 9.4
600	- 4.7	0.7
550	-10.4	6.5
500	6.5	- 6.8
450	19.1	-10.4
400	3.6	- 3.6
350	- 9.0	54.7
300	8.3	41.4
250	43.6	-10.4
200		

Table 7. Average computed advective temperature tendency. 0300 GMT 10 Feb. - 1500 GMT 18 Feb. 56 for Lihue.

STABILITY

Figures 7-9 represent time sections of virtual-equivalent-potential temperatures over Lihue for three selected periods. The occurrence of electrical activity at Lihue during these periods is marked on the lower portions of the diagrams. The significance of these diagrams is found in the fact that convective instability is nearly always present in the air mass over the Hawaiian Islands. The convective instability usually results because of the moisture distribution. Abundant moisture present in the lower levels normally decreases rapidly with height.

Attempts at correlating electrical activity with the axes of the minima of virtual-equivalent-potential temperature, or the maximum height of the convectively unstable layer, were unsuccessful. Attempts to correlate thunderstorms with the vertical gradient of virtual-equivalent-potential temperature or with specific minimum values of virtual-equivalent-potential temperature were similarly unsuccessful.

Graphical computations on thermodynamic charts show that small lifts, usually 100 mb or less, of the layers below 700 mb are more than sufficient to release the potential instability. Mechanical lifting of these magnitudes can easily be realized over the mountain ranges of Kauai and Oahu, ranging up to 4500 feet above sea level. Why is it that more thunderstorms do not occur with conditions so

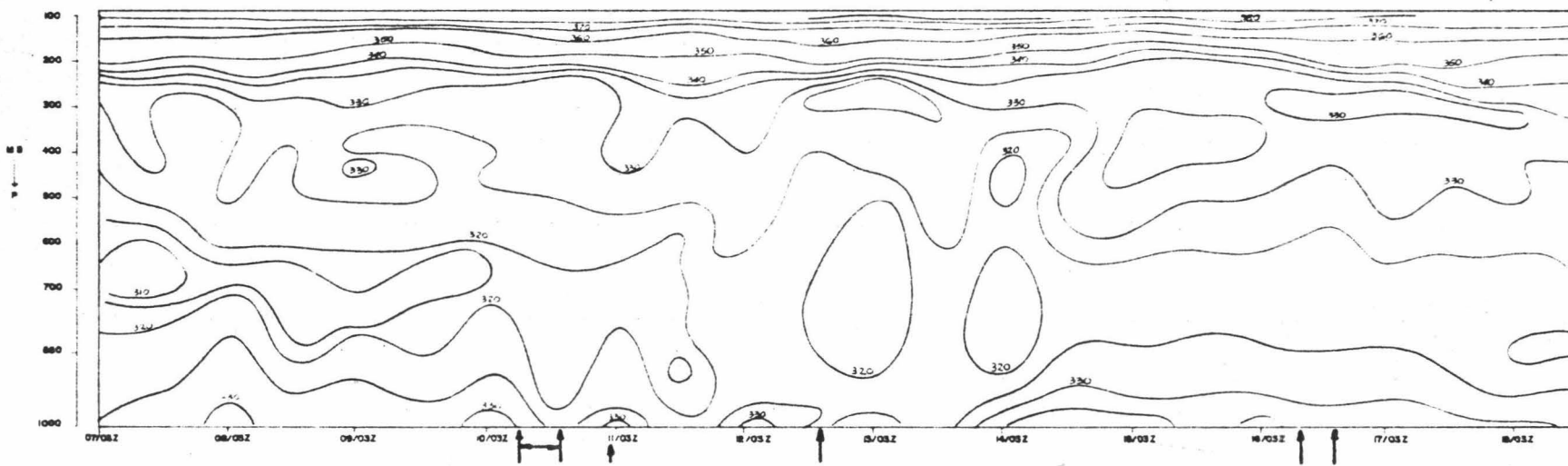


Fig. 7. Virtual-equivalent-potential temperature, $^{\circ}\text{K}$ Lihue Feb. 1956
 Thunderstorm occurrences marked by arrows.

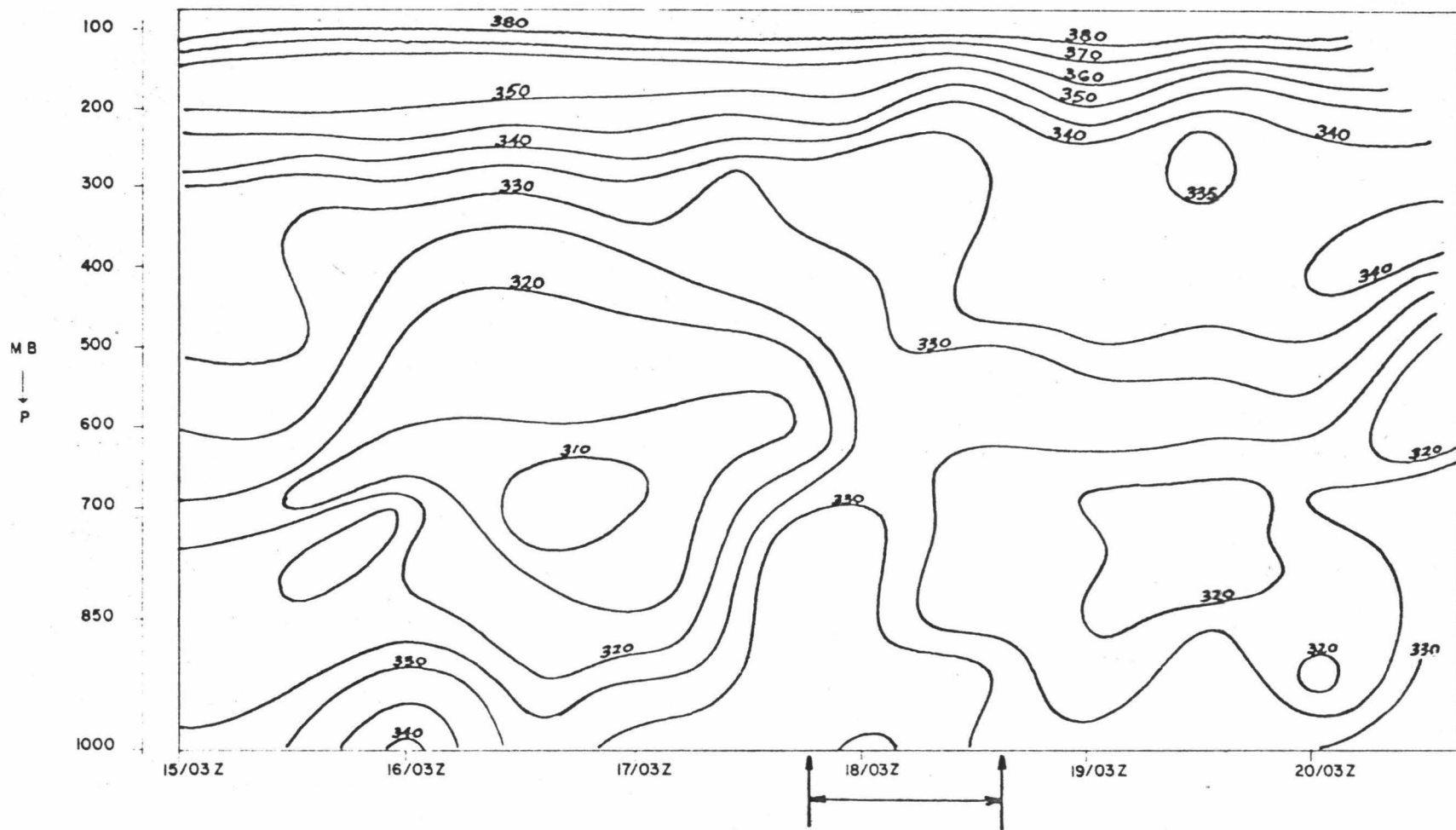


Fig. 8. Virtual-equivalent-potential temperature, °K Lihue Jan. 1957
Thunderstorm occurrences marked by arrows.

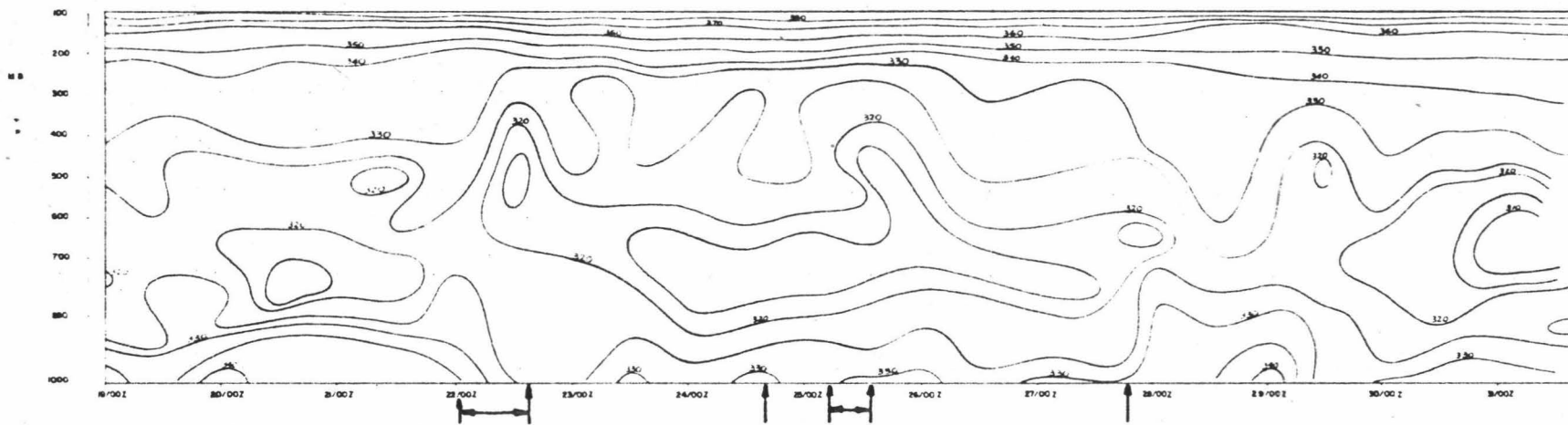


Fig. 9. Virtual-equivalent-potential temperature, $^{\circ}\text{K}$ Lihue Jan. 1962
 Thunderstorm occurrences marked by arrows.

suitable for their development? The absence of more frequent and severe convective activity demonstrates that the latent instability is not being released by simple orographic lift.

RELATIVE HUMIDITY

Figures 10-12 represent time sections of relative humidity for the same periods shown in Figs. 7-9. Electrical activity at Lihue is shown on the lower portions of the diagrams. These diagrams show systematic variations of moisture with periods of two to three days.

Figure 10 shows that prolonged thunderstorm activity at Lihue commencing 0800 GMT 10 Feb 56 and continuing through 1700 GMT was preceded by increasingly higher values of relative humidity (RH) beginning about a day and a half prior to the onset of thunderstorms.

Similarly, continuous thunderstorm activity at Lihue began on 2200 GMT 17 Jan 57 and continued through 1800 GMT 18 Jan. Fig. 11 reveals a sharp trend towards increasing values of relative humidity with time and height commencing about 2100 GMT 16 Jan or nearly a full day prior to the onset of thunderstorms.

The same feature can be noted at 0000 GMT 21 Jan 62 (Fig. 12) which preceded the continuous activity at Lihue commencing 0100 GMT 22 Jan and continuing through 1500 GMT.

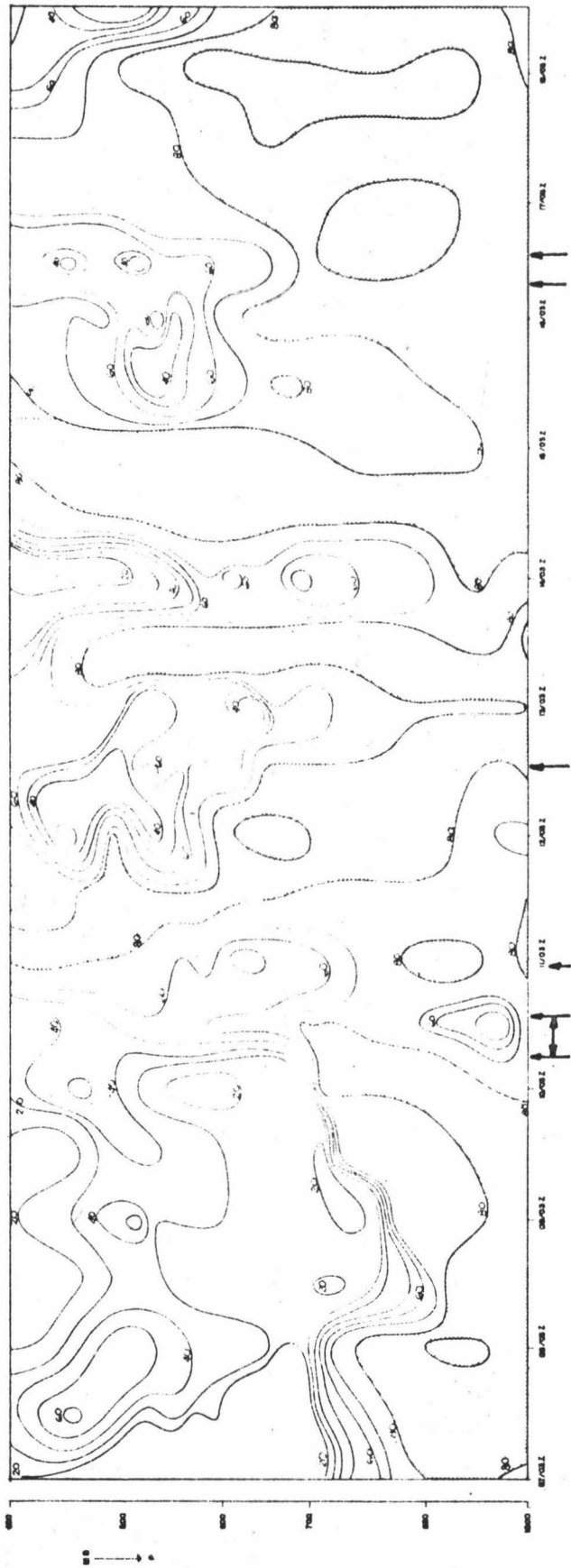


Fig. 10. Relative humidity - % Lihue Feb. 1956
Thunderstorm occurrences marked by arrows.

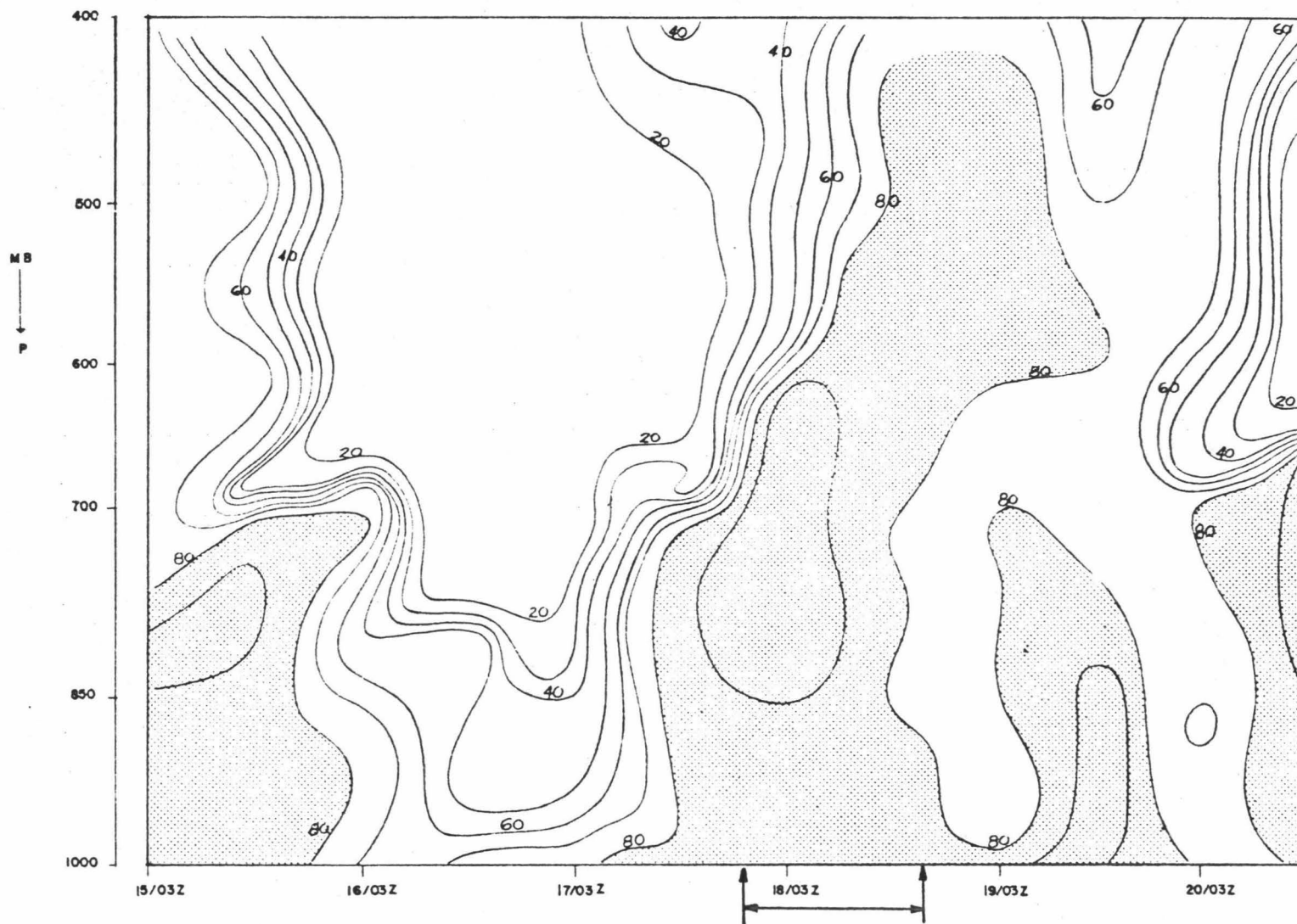


Fig. 11. Relative humidity - % Lihue Jan. 1957
Thunderstorm occurrences marked by arrows.

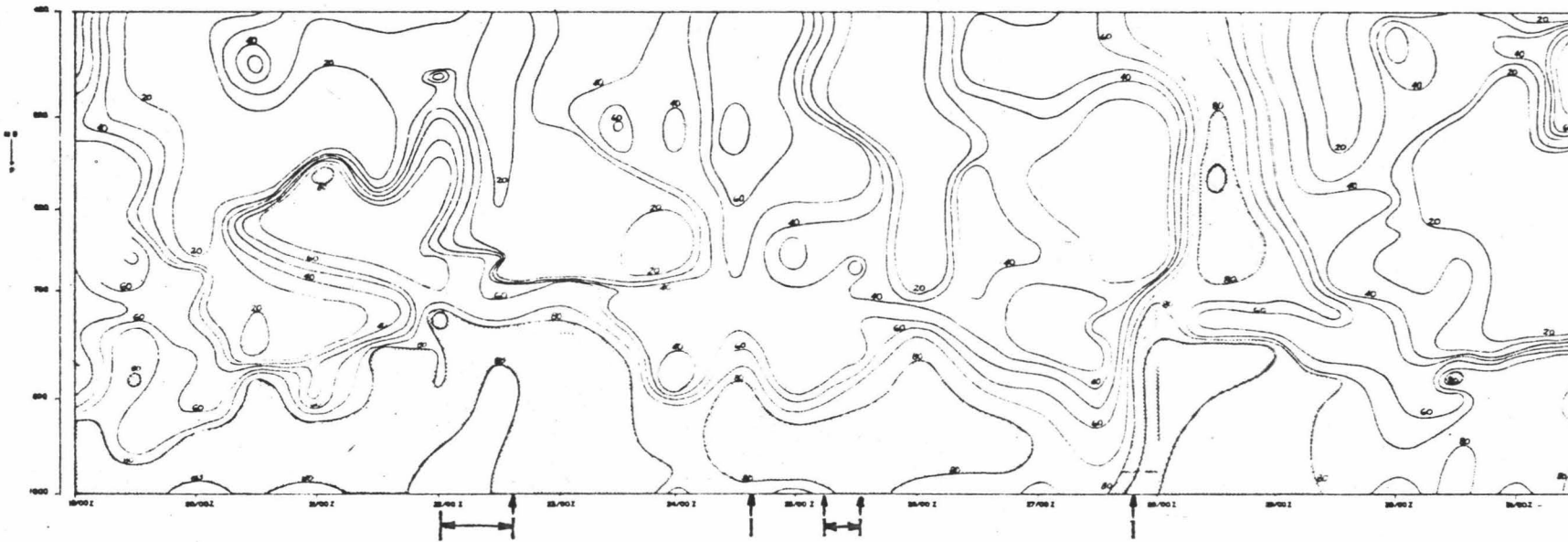


Fig. 12. Relative humidity - % Lihue Jan. 1962
 Thunderstorm occurrences marked by arrows.

The patterns were not entirely consistent, however. Increasing values of RH subsequent to 0300 GMT 13 Feb 56 did not culminate in significant thunderstorm development at Lihue despite a deep moist layer extending to over 500 mb twelve hours later.

Relative humidities were usually high during thunderstorm activity. One exception worthy of note is the relative minimum in the low levels centered on 1500 GMT 10 Feb 56. As observed previously, thunderstorms prevailed nearly continuously from 0800-1700 GMT. It could be argued that the low level RH minimum resulted from the desiccating effects produced by downdraft motion as thunderstorms were in progress at the time the sounding was made. However, inspection of the hourly records at Lihue provided no substantiating evidence of gusty downdraft conditions during the period.

In routine forecasting use of auxiliary charts such as RH diagrams is prohibited by the difficulty of objectively determining the trend of the pattern, which is essentially a problem involving a second order prognostic equation. A second difficulty is in recognizing whether the changes represent responses due to horizontal advection of moisture or those due to lifting of moisture from lower levels as a result of vertical motions.

PHYSICAL MODELING

A physical cloud model designed for computer application has been developed by Weinstein (1966). The model simulates steady state cumulus convection.

The three basic equations of the model, energy thermodynamic, and moisture equations, yield steady state profiles of vertical motion, cloud temperature, temperature excess of cloud over environment, cloud mixing ratio, and liquid water content of the cloud. The printed output also yields maximum cloud top, amount and duration of rainfall, and updraft area at various stages of development.

Input to the model consists of a sounding of pressure, temperature, relative humidity, and wind (optional) at all mandatory and significant levels. An assumed cloud base height and updraft radius are additional input parameters.

The entrainment parameter is assumed to be

$$\mu = \frac{.2}{R} \quad (10)$$

The model is similar, and the entrainment rate identical, to the plume model considered by Squires and Turner (1962). Morton's (1960) values of the entrainment constant with cylindrical profiles has been slightly modified from 0.116 to 0.10 in Weinstein's model.

The model is sufficiently versatile to incorporate many options of development. In addition to those already mentioned the ice nucleation temperature, effects of wind

shear, autoconversion and accretion exchange rates, buoyancy reduction, updraft radius, and initial impulse at cloud base may be initially specified to simulate various conditions.

The ice nucleation temperature is initially specified to simulate spontaneous (248 °K) or artificial nucleation (267 °K).

The effect of wind shear as a mixing and shearing agent modifying vertical growth can be included as part of a subroutine or it can be omitted.

The autoconversion rate specifies the rate at which cloud water is converted to hydrometeor water and the accretion rate determines the rate at which hydrometeors collect water. Both can be varied to simulate various degrees of efficiency.

Cloud buoyancy, used to determine the vertical velocity, must be reduced by the weight of the liquid water carried aloft. The options provided in the program allow for buoyancy retardation by cloud and hydrometeor water or by cloud water alone.

The updraft radius alternately can be kept constant or allowed to vary according to the mass continuity equation. As the vertical velocity increases/decreases with height, the updraft area decreases/increases.

Figure 13 depicts the basic flow diagram used in the model.

1. The model interpolates the initial input sounding for constant height increments of 200 meters.
2. The standard parcel method, with mixing or entrainment, is numerically simulated by the program. The parcel ascends one height increment and is then mixed with the environment at constant pressure.
3. The cloud and hydrometeor water are computed next. The vertical velocity is then computed as the buoyancy less the drag created by the liquid water carried and mixing with the slower environmental air.
4. Calculations for the next higher height interval are again computed provided that the cloud temperature is greater than the ice nucleation temperature. The ice nucleation temperature is specified initially, corresponding to spontaneous or artificial nucleation. If the cloud temperature is less than that of the ice nucleation temperature, the liquid water is frozen and the latent heat gain is added to the computations performed for the next height increment. This increase in energy is added for one step only; thereafter calculations are performed with respect to ice saturation.

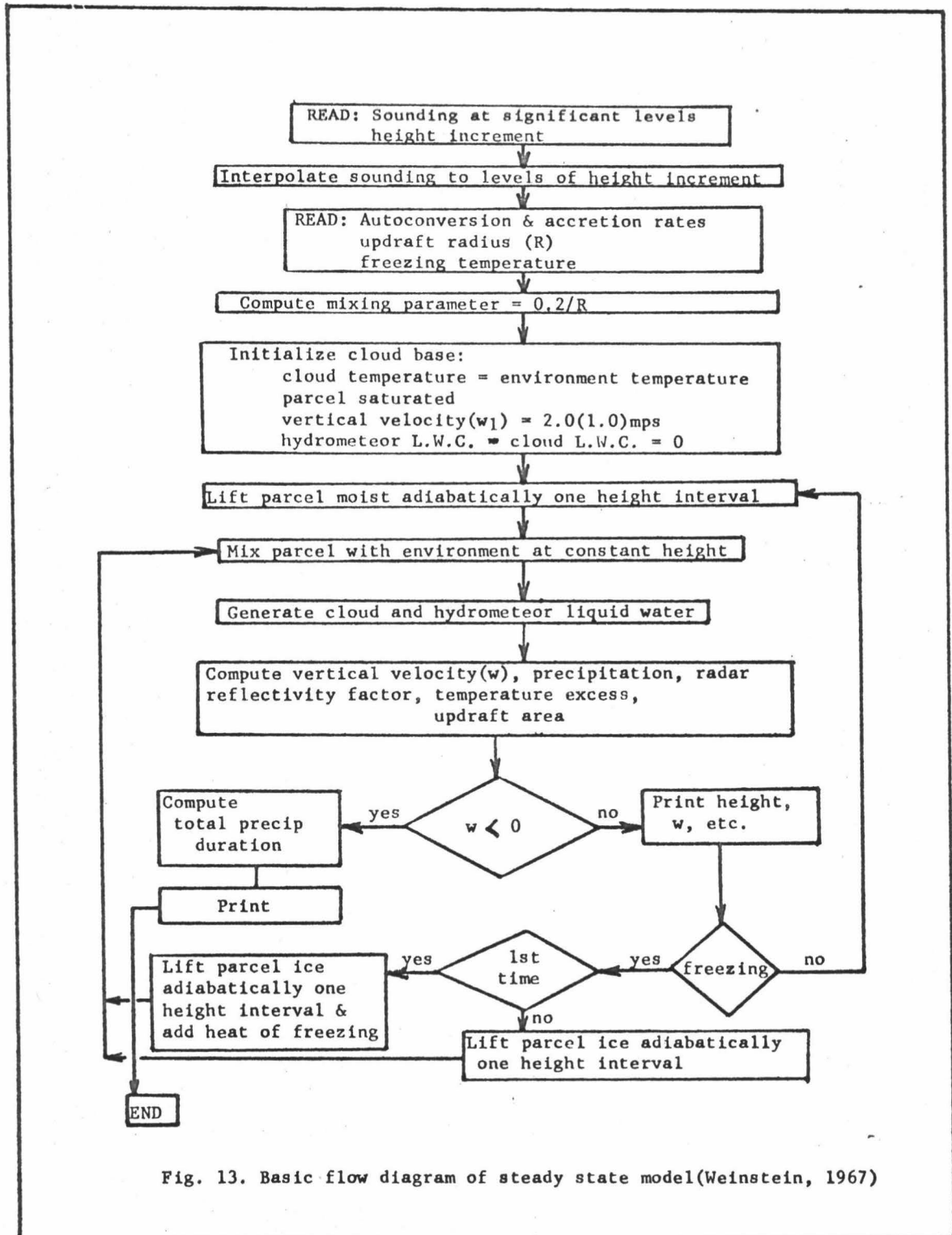


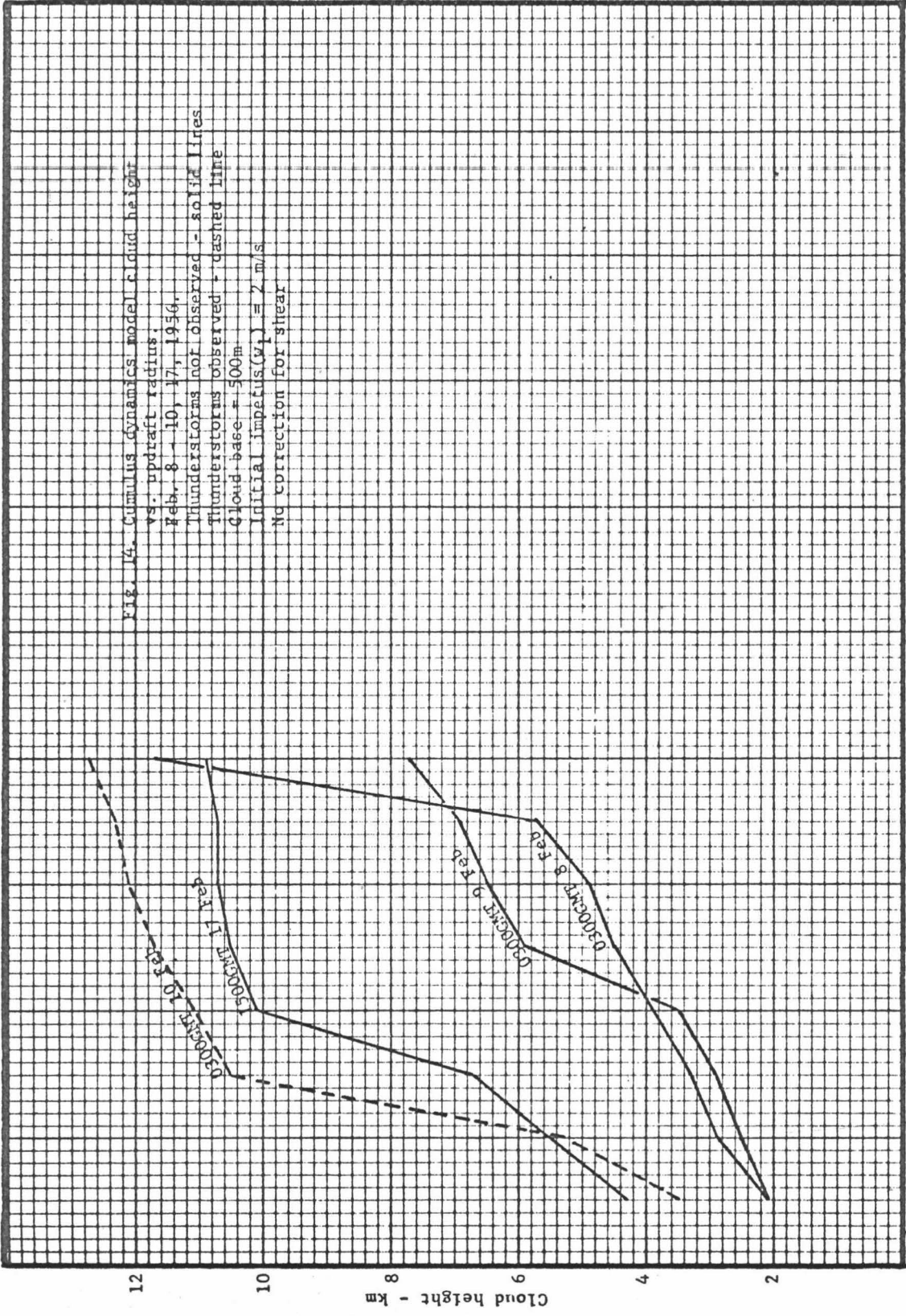
Fig. 13. Basic flow diagram of steady state model(Weinstein, 1967)

5. The computations continue stepping for 200 meter height intervals until downward vertical motions, indicating negative buoyancies, have been computed.

Figures 14-17 show some of the results of the model, tested with a few of the options. The data used were taken from selected dates for the same periods shown in Figs. 7-9. The spontaneous ice nucleation temperature was used in all runs.

Effective discrimination of the period of activity on 10 Feb 56 from the lack of any activity on the 8th and 9th is shown in Fig. 14. Computed cloud heights for the 10th were significantly higher than those computed for the 8th or 9th for all updraft radii. The largest difference, about 8 km, occurs for an updraft radius of 1.5 km between the 8th and 10th. The model was not particularly successful in discriminating the lack of activity on the 17th from that of the 10th. Computed cloud heights for the 17th, although generally lower than for the 10th, were quite similar. There is, however, a significantly large difference of about 4 km for an updraft radius of 1.5 km. For updraft radii less than or exceeding 1.5 km the differences were less substantial.

Figure 15a shows good correspondence for the prolonged thunderstorm activity that began on 2200 GMT 17 Jan 57 and continued through 1800 GMT 18 Jan. The computed cloud heights from the 1500 GMT 17 Jan sounding do not differ



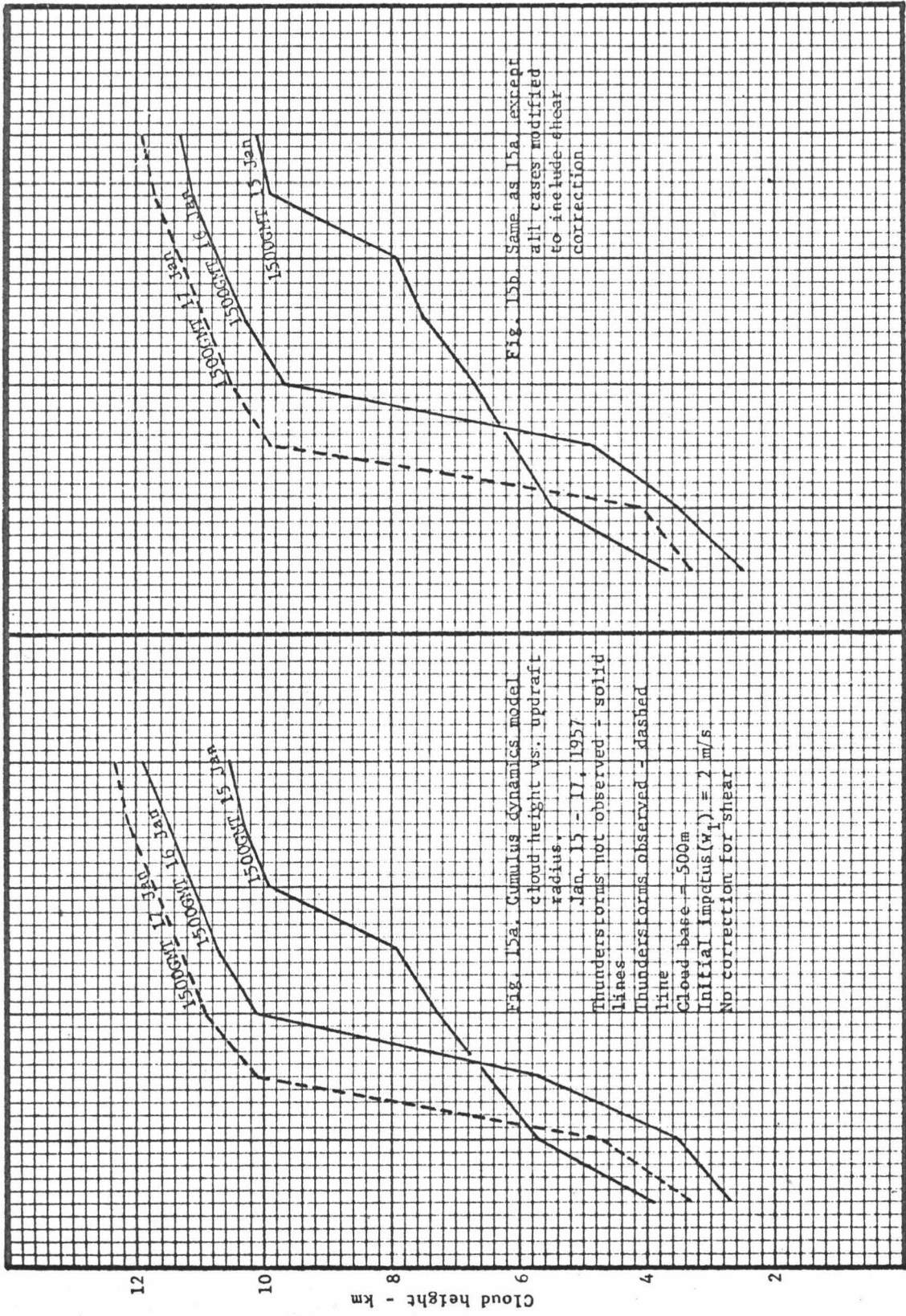
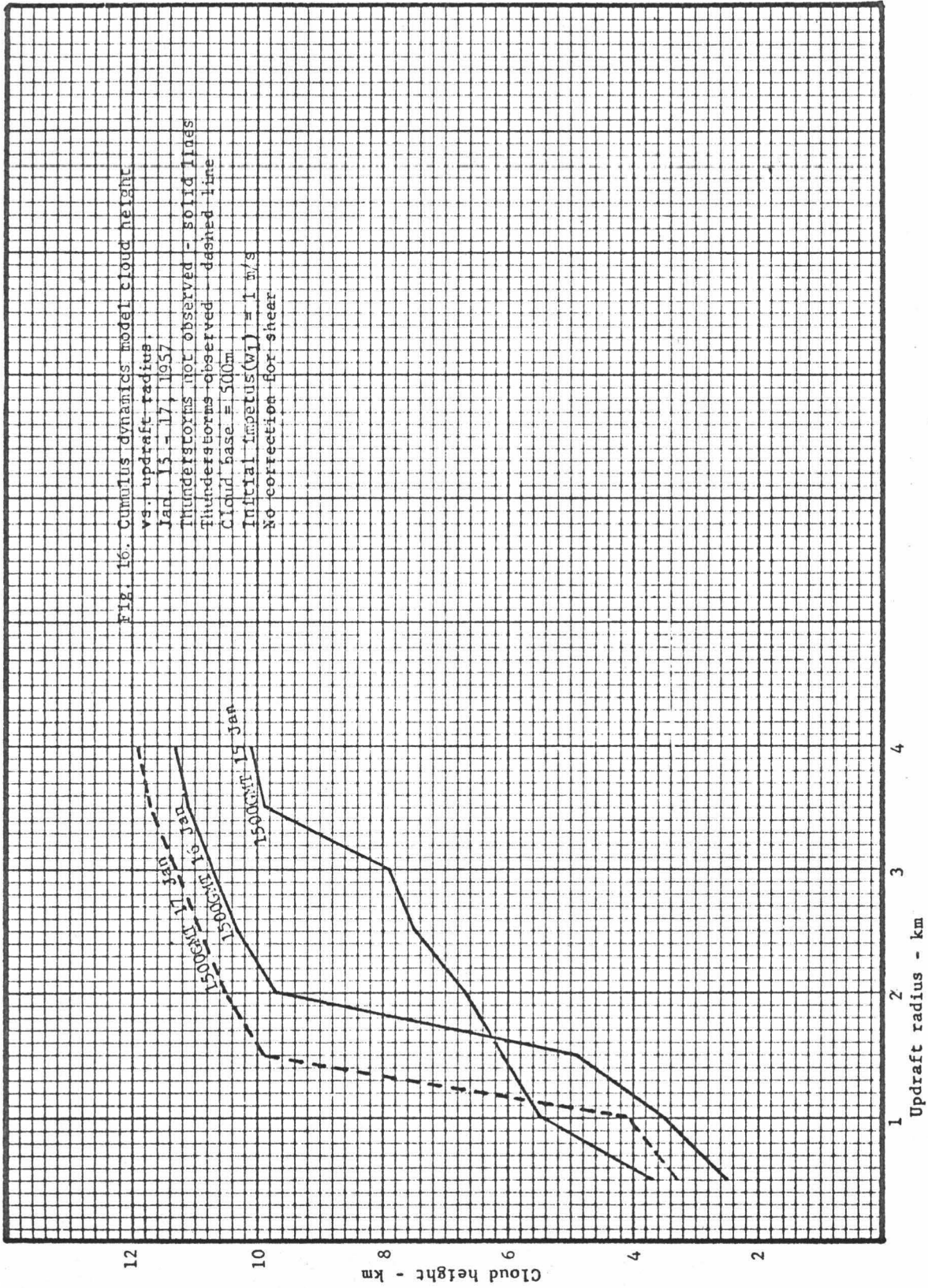
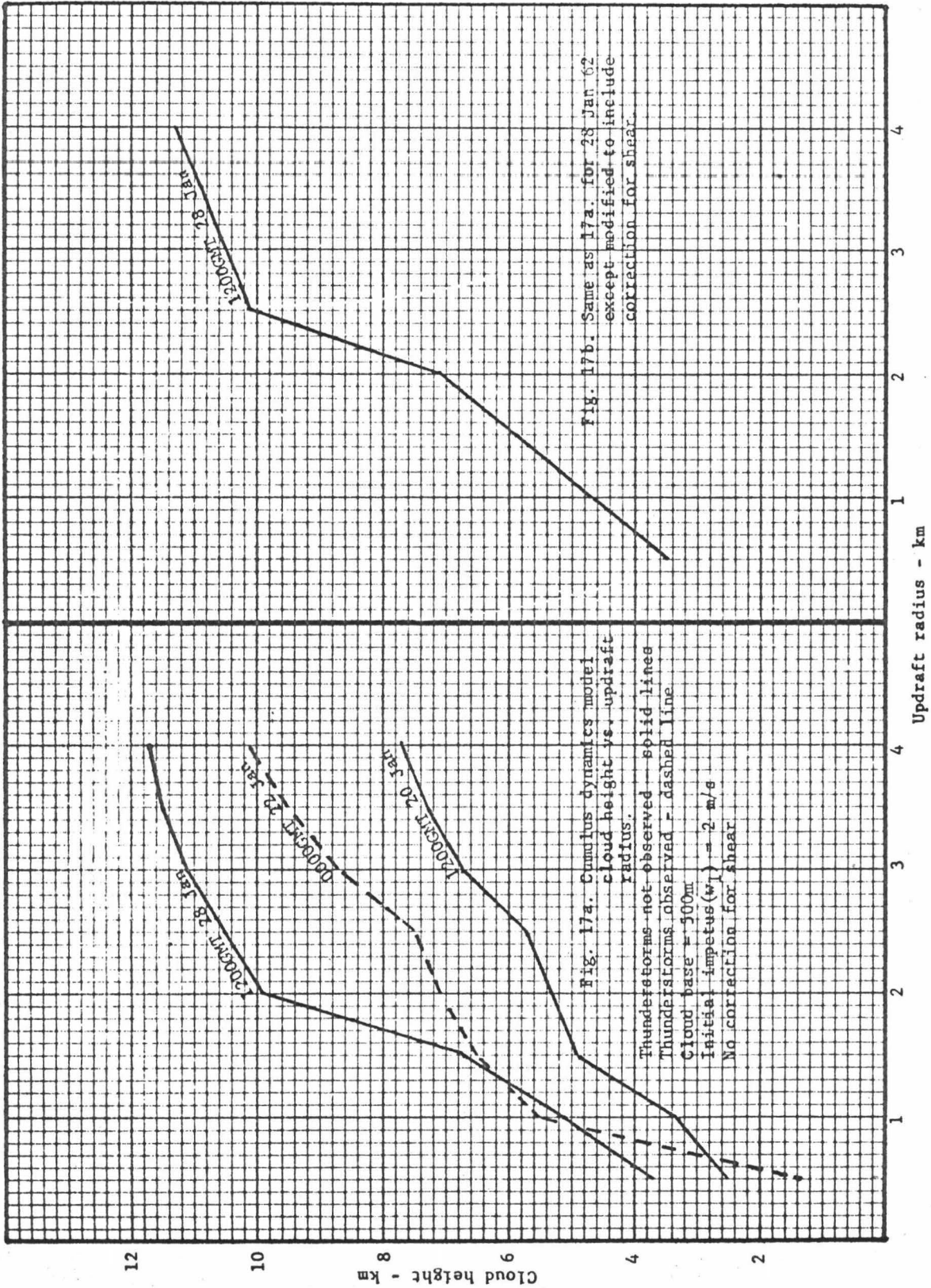


Fig. 15a. Cumulus dynamics model cloud height vs. updraft radius. Jan. 15 - 17, 1957. Thunderstorms not observed - solid lines. Thunderstorms observed - dashed line. Cloud base = 500m. Initial impetus (w_1) = 2 m/s. No correction for shear.

Fig. 15b. Same as 15a except all cases modified to include shear correction.

Fig. 16. Cumulus dynamics model cloud height vs. updraft radius. Jan. 15 - 17, 1957. Thunderstorms not observed - solid lines. Thunderstorms observed - dashed line. Cloud base = 500m. Initial impetus (w_1) = 1 m/s. No correction for shear.





significantly from those computed from the 1500 GMT 16 Jan sounding, however, except for an updraft radius of 1.5 km. The difference in the computed cloud heights for an updraft radius of 1.5 km for the two dates is about 4.5 km. The model was moderately successful in discriminating the lack of activity on the 15th, especially for updraft radii from 1.5-3.0 km. However, the results are inconclusive for radii less than 1.5 km or greater than 3.0 km.

Figure 15b represents the same dates and input parameters as Fig. 15a except that the effects of wind shear have been considered in the computations. This modification is observed to provide an inhibiting effect. All computed cloud heights for all dates are lower than those computed without considerations of wind shear. In spite of large differences in shear at levels above 300 mb for the three dates (Tables 8-10), the general configurations are unchanged from those in Fig. 15a and the modification failed to provide further discrimination.

Figure 16 again represents the same dates and input parameters as Fig. 15a. No shear correction has been included. However, the initial impetus at the cloud base has been modified from two m/s to one m/s. It is again observed that the modification tends to decrease the computed cloud heights from those in Fig. 15a. Again, however, the general configurations and relative placements of the distributions have not changed significantly. The

P(mb)	T(°C)	RH(%)	V(mps)
950	18.7	82	180/06
850	11.7	85	240/09
795	9.7	91	240/09
707	3.5	74	240/10
700	3.3	58	270/11
682	2.5	22	270/10
668	1.7	54	270/10
618	- 2.7	82	270/10
600	- 3.2	66	270/10
570	- 6.5	59	270/10
500	-11.2	72	270/09
472	-13.5	69	270/10
418	-20.5	28	270/15
400	-22.0	18	270/22
300	-37.1	20*	280/47
250	-41.1	20*	280/50
200	-52.1	20*	280/40
150	-64.9	10*	280/40
100	-75.0	10*	280/30

* assumed values

Table 8. Input parameters for cumulus dynamics model calculations 1500 GMT 15 Jan. 57.

P(mb)	T(°C)	RH(%)	V(mps)
950	20.0	48	260/06
932	19.0	42	260/08
850	13.5	52	260/06
800	10.0	52	260/08
772	9.0	22	260/09
700	6.7	13	240/10
500	-11.7	16	230/09
400	-25.3	19	260/10
300	-38.3	22	260/15
250	-42.9	20*	260/15
200	-53.8	20*	260/15
150	-64.0	10*	260/15
100	-74.2	10*	260/15

* assumed values

Table 9. Input parameters for cumulus dynamics model calculations 1500 GMT 16 Jan. 57.

P(mb)	T(°C)	RH(%)	V(mps)
950	19.6	82	200/07
850	13.7	86	180/07
765	5.4	80	190/08
700	5.7	50	190/10
685	5.5	22	190/09
675	4.5	32	190/09
655	3.5	20	190/09
500	-12.7	16	240/20
400	-24.9	48	260/24
300	-39.8	22	260/32
250	-44.9	20*	260/30
200	-54.2	20*	260/30
150	-64.0	10*	260/30
100	-70.7	10*	260/30

* assumed values

Table 10. Input parameters for cumulus dynamics model calculations 1500 GMT 17 Jan. 57.

modification was not successful in producing further discrimination.

The results shown in Fig. 17a indicate the model was particularly unsuccessful in discriminating the activity on 22 Jan 62 from the lack of any activity on the 28th. This is also true, though less conclusively, for the period of inactivity on the 20th.

Figure 17b represents the computed cloud heights for the 28th modified to include the effects of shear. Except for lowering the individual cloud heights slightly, the modification produced no significant changes in the results.

The results of these first tests of the model, seen in Figs. 14-17, are generally inconsistent. While the model verified the most severe occurrences, it over predicted cloud heights for those dates on which no thunderstorms occurred. The model appears to discriminate most effectively for updraft radii of 1.5 km. Interestingly, while Byers (1965) and Byers and Braham (1949) observed in their thunderstorm project that the radar cloud associated with a single thunderstorm cell was about six to ten km in diameter, aircraft measurements showed the modal width of updraft and downdraft area to be approximately 1.5 km.

In summary, Figs. 14-17 show the model was able to separate the most extreme cases. However, the model is ineffective in discriminating between nearly identical thunderstorm and non-thunderstorm soundings. In addition,

the model is apparently insensitive to the effects of wind shear or variations of the initial impetus. The shortcomings of the model will need to be subjected to closer analysis and more comprehensive tests. Some of the limitations of the model are due to the fact that it does not account for vertical exchange of moisture or evaporation of rainfall. In defense of the model, it must be pointed out that the small number of tests made so far are too few to reach a general conclusion regarding its reliability.

CONCLUSIONS

The thunderstorm frequencies shown in Figs. 1-3 are based only on data gathered from the four first-order Weather Bureau stations at Lihue, Honolulu, Kahului, and Hilo. Bias certainly results from the fact that observations at these airport sites cannot be completely representative of conditions throughout the remaining portions of their respective islands. Evidence of the non-representativeness of the airport observations is often observed in the wide range of weather conditions reported by military, Weather Bureau, and cooperative weather observers on various areas of the same island. Within the limitations of the data, however, the study has shown that thunderstorms are only poorly correlated with major synoptic systems. On a practical basis, this fact suggests that thunderstorms should only be forecast when other supporting evidence,

such as radar reports, satellite photos, observations, etc., indicate prior existence of thunderstorms.

Regarding the observed semi-diurnal frequency of thunderstorms, no evidence has been presented to support low-level warm advection as a mechanism to explain the nocturnal thunderstorm maxima in the Hawaiian Islands. Such a mechanism had been proposed by Means (1944) to explain the nocturnal thunderstorm maximum over the mid-western United States. Similarly, no evidence has been presented that large-scale disturbances maintain periodic tendencies corresponding to the observed semi-diurnal thunderstorm frequencies. On the other hand, insolation and cloud radiation, because of their periodic character, can at least qualitatively support the observed frequencies. Cloud radiation is a prominent factor to be considered in future work but the difficulty of obtaining precise and timely measurements likely preclude much study of this important area.

Results of the study have shown that radiative transfer and vertical motions are dominant energy processes controlling convective activity in the Hawaiian Islands. Vertical motion is apparently the most effective destabilizing influence.

The study has shown that, although the air mass over the Hawaiian Islands is nearly always convectively unstable, the convective instability is inefficiently released and the triggering mechanism for release is only poorly under-

stood. The fact that many thunderstorms occur during ostensibly quiescent periods (i.e., tradewind patterns) may partially be explained by topographic lifting releasing the ever present convective instability. However, the lack of more frequent convective storms suggest that mechanical lifting over the mountains is often suppressed by strong subsiding motions above the mountains. With strong flow up and over the mountains, strong horizontal divergence can be expected on the windward side such that ascending motion reverses with height to descending motions at elevations above the mountain tops.

The purpose of this study has been partially attained. It has shown that the convective instability is sometimes released by frontally induced low level convergence. At other times, the release of convective instability is achieved by friction induced low level convergence or differential advection associated with cyclonic circulations. At still other times, the convective instability is released by topographic lifting. In addition, results of the cloud model have shown that entrainment is a necessary but not sufficient condition to explain the relatively infrequent occurrence of thunderstorms. Sufficient groundwork has now been established to provide more penetrating attacks on the problem with the prospect of gaining fruitful and positive results.

RECOMMENDATIONS

It is recommended that an additional study be made of observations from cooperative weather observers and military weather units. Such a study should reveal an increase in the number of thunderstorm-days. The study should be used to modify the results presented in this paper.

It is further recommended that the Penn State cumulus dynamics model be tested on a daily operational basis. The model has shown some promise but completely realistic results cannot be expected from the model, mainly because all tests have considered only a static environment. More experience and future modifications of the program, including the effects of a non-stationary environment, may yield more realistic and productive results. While serving as another forecast tool, additional statistics may be helpful in modifying the program. It is also recommended that a study be made of additional parameters, such as subsidence over the mountains, and the results used to modify the numerical model.

Table 11. Input parameters for cumulus
dynamics model calculations
0300 GMT 8 Feb. 56.

P(mb)	T(°C)	RH(%)
950	17.3	80
900	14.0	83
850	11.8	79
800	9.7	66
750	7.1	59
722	5.7	71
700	5.5	13
690	4.0	20
658	1.0	21
650	1.6	14
643	0.5	39
600	-2.7	14
550	-7.2	15
500	-12.4	16
450	-18.5	17
438	-20.0	28
400	-25.5	19
350	-33.8	29
300	-43.0	20*
250	-51.7	20*
200	-51.8	20*
175	-55.1	10*

Table 11 (cont.)

P(mb)	T(°C)	RH(%)
150	-63.2	10*
125	-67.6	10*
100	-75.3	10*

* assumed values

Table 12. Input parameters for cumulus
dynamics model calculations
0300 GMT 9 Feb. 56.

P(mb)	T(°C)	RH(%)
950	18.4	82
900	15.8	78
850	13.1	73
800	10.3	68
783	11.0	25
760	10.5	19
750	9.8	19
700	5.9	24
650	1.9	27
600	-2.4	30
550	-7.1	31
530	-9.0	31
515	-10.3	51
500	-11.3	49
450	-15.9	30
435	-17.2	26
400	-23.1	18
350	-30.5	20
300	-38.7	22
250	-48.4	20*
200	-57.6	20*
175	-61.7	10*

Table 12 (cont.)

P(mb)	T(°C)	RH(%)
150	-66.2	10*
125	-71.2	10*
100	-75.0	10*

* assumed values

Table 13. Input parameters for cumulus dynamics model calculations 0300 GMT 10 Feb. 56.

P(mb)	T(°C)	RH(%)
950	18.8	80
900	15.2	83
850	12.2	82
800	9.3	80
750	5.7	81
715	3.0	82
700	4.4	32
650	0.7	26
600	-3.4	14
550	-7.8	15
530	-9.0	24
500	-13.9	38
458	-19.0	53
450	-20.0	50
400	-26.9	32
350	-33.2	50
335	-34.7	18
300	-41.7	20*
250	-48.9	20*
200	-56.6	20*
175	-61.3	20*

Table 13 (cont.)

P(mb)	T(°C)	RH(%)
150	-66.1	20*
125	-70.1	10*
100	-72.6	10*

* assumed values

Table 14. Input parameters for cumulus dynamics model calculations 1500 GMT 17 Feb. 56.

P(mb)	T(°C)	RH(%)
950	18.4	84
900	15.1	86
850	11.6	88
800	9.0	89
750	6.6	88
700	3.4	89
650	-0.9	92
638	-1.3	91
613	-1.7	87
600	-2.9	84
550	-7.0	79
500	-11.6	74
450	-16.8	70
400	-23.5	70
360	-29.9	41
350	-31.1	40
304	-38.5	36
300	-39.9	22
250	-41.1	20*
200	-50.0	20*
175	-56.1	10*

Table 14 (cont.)

P(mb)	T(°C)	RH(%)
150	-63.0	10*
125	-69.6	10*
100	-77.0	10*

* assumed values

Table 15. Input parameters for cumulus dynamics model calculations 1200 GMT 20 Jan. 62.

P(mb)	T(°C)	RH(%)
950	19.0	82
900	15.3	83
850	11.6	84
820	9.3	80
810	8.1	66
792	8.1	22
778	12.0	17
717	7.2	23
700	6.1	26
607	-4.5	69
588	-2.7	22
547	-3.0	15
500	-9.3	15
479	-12.8	25
447	-16.8	53
408	-19.8	25
400	-19.9	17
300	-36.0	21
250	-46.3	20*
200	-57.0	20*

Table 15 (cont.)

P(mb)	T(°C)	RH(%)
150	-66.4	10*
100	-76.3	10*

* assumed values

Table 16. Input parameters for cumulus dynamics model calculations
0000 GMT 22 Jan. 62.

P(mb)	T(°C)	RH(%)
950	17.7	76
850	13.2	82
755	6.0	87
732	6.0	64
700	4.7	69
690	3.5	55
670	1.5	24
660	0.0	53
610	-4.0	23
500	-13.3	50
400	-23.2	40
300	-37.6	67
250	-47.0	20*
200	-59.0	20*
150	-65.1	10*
100	-72.7	10*

* assumed values

P(mb)	T(°C)	RH(%)	V(mps)
950	19.3	84	230/14
900	16.0	87	230/15
850	12.8	89	240/17
780	8.3	95	240/18
752	4.0	63	240/19
745	4.3	48	240/20
721	5.4	69	240/21
700	4.4	74	240/22
562	-4.8	94	260/26
500	-10.5	81	270/31
432	-17.7	70	280/30
400	-22.5	66	280/29
358	-28.5	63	300/40
300	-36.4	46	320/51
271	-40.0	36	320/51
250	-44.4	20*	310/52
200	-54.4	20*	310/48
150	-66.0	10*	300/50
100	-72.5	10*	290/36

* assumed values

Table 17. Input parameters for cumulus dynamics model calculations 1200 GMT 28 Jan. 62.

APPENDIX

List of Symbols

α	proportionality constant
c_p	specific heat of humid air at constant pressure
$\bar{\nabla}_p$	del operator in a p-system
ϵ	0.622
e	base of natural logarithms; saturation vapor pressure
F	black-body radiation
f	Coriolis parameter
γ_d	dry adiabatic lapse rate
γ	lapse rate
L	latent heat of evaporation
μ	entrainment parameter
q	heat per unit mass
p	pressure
p_1	pressure at bottom of layer
p_2	pressure at top of layer
R	gas constant for dry air
ρ	density
θ	included angle between V_1 and V_2
T	temperature
t	time
\bar{V}_g	geostrophic mean vector wind
V_1	absolute value of wind at p_1
V_2	absolute value of wind at p_2
ω	mixing ratio
w	vertical velocity

65

BIBLIOGRAPHY

- Byers, H. R., 1965: Elements of Cloud Physics, Univ. of Chicago Press, Chicago, Ill., 185 pp.
- Byers, H. R., and Brahama, R. R., Jr., 1949: The Thunderstorm (Washington: U. S. Weather Bureau).
- Lee, C. B. H., 1967: Weather Phenomena in Hawaii, Part II, Final Rept., Contract Cwb 11373, Hawaii Inst. of Geophys., Univ. of Hawaii, 41-53.
- Means, L. L., 1944: The nocturnal maximum of thunderstorms in the midwestern states, Misc. Rept. No. 16, Univ. Chicago, 38 pp.
- Morton, B. R., 1960: J. Fluid Mech., 9, 107.
- Squires, P., and Turner, J. S., 1962: Tellus, 14, 422.
- Weinstein, A. I., 1966: Steady State Cumulus Dynamics Model. Technical Rept. No. 15, NSF-GP-4743, Dept. of Meteorology, The Pennsylvania State Univ., University Park, Pa., 18 pp.
- Worthley, L. E., 1967: Weather Phenomena in Hawaii, Part I, Final Rept., Contract Cwb 11373, Hawaii Inst. of Geophys., Univ. of Hawaii, 1-39.
- Yeh, T. C., C. C. Wallen, and J. E. Carson, 1951: A study of rainfall over Oahu. Meteo. Monogr.